Advantageous Exploitation of Characteristic Modes Analysis for the Design of Three Dimensional Null Scanning Antennas

Francesco Alessio Dicandia, *Student Member, IEEE,* Simone Genovesi, *Member, IEEE,* and Agostino Monorchio, *Fellow, IEEE*

***Abstract*—A novel design strategy for realizing three dimensional null-scanning antennas by resorting to the Characteristic Modes Theory is described. By exploiting the variation of the excitation degree of the current modes (J_n) over the investigated platform, a null of the pattern can be placed in any desired direction in the upper hemisphere. A rectangular conductive plane has been taken into account as test case to validate the design strategy. Design guidelines are provided for selecting and placing the proper exciters in order to realize the suitable excitation of the current. Measurements on a realized prototype are in good agreement with simulations confirming the reliability of the proposed approach.**

***Index Terms*—Characteristic Modes, Pattern reconfigurable, null-scanning.**

I. Introduction

In the last years, the use of reconfigurable antennas is gaining more and more attention since they can enhance the modern radio-frequency (RF) front-ends and thus improving the overall wireless communication system performance [1]. An antenna can be considered reconfigurable when it is able to modify its radiative proprieties such as the frequency band of operation [2], [3], the exhibited polarization [4] or the radiation pattern shape [5]. Depending on their degree of reconfigurability, these antennas may support more than one wireless communication standard or decrease the front end processing by providing filtering features/capability [1]. Pattern reconfigurable antennas are commonly employed to increase spectral efficiency guaranteeing, at the same time, a higher level of reliability of the overall radio communication link. Indeed, by properly modifying the radiation pattern, it is possible to cope with the environment impairments and establish a steady link between the transmitter and the receiver. Moreover, pattern reconfigurable antennas may reduce the effect of the interferences by placing a null of the pattern in the direction of the intentional or casual disturbance and so improve the signal-to-interference ratio (SIR) and the system performance [6]. Several approaches have been proposed to realize pattern reconfigurable antennas. For instance, in [7] an aperture coupled driven patch with a parasitic layer composed of 3 × 3 square shaped metallic pixels connected by pin diodes is proposed to realize a beam steering antenna. In [8] a reconfigurable antenna able to switch between the monopole-like pattern and broadside pattern is presented.

A null-steering capability is reported in [9] and [10] where a patch antenna employing twelve varactors realizes the null-steering along one principle plane and in a limited three-dimensional range, respectively. In [11] a null-steering antenna working at 2.4 GHz is obtained by employing a shorted patch. Moreover, a two-port null-steering antenna in circular polarization (CP) is proposed for GPS systems in [12].

Over the past years, the Characteristic Modes Theory (CMT) [13], [14] has received a renewed and significant interest in the field of the antenna design for several applications. Indeed, the CMT allows a meaningful insight of the scattering and radiation proprieties of a structure, based only on its geometry and regardless of the feeding arrangement. For instance, some multiple-input-multiple-output (MIMO) antennas exploiting the CMT are proposed in [15]–[19]. Antennas on complex platform have also benefited from the CMT [20]–[22].

The purpose of this paper is to propose a three dimensional null-scanning antenna by exploiting all the potential of the phase-shifted Characteristic Modes (CMs) approach [23]. The proposed antenna consists of a rectangular conductive body, properly stimulated by four capacitive coupling exciters (CCEs) [24], [25]. The rectangular conductive plate acts as the main radiator, whereas the four CCEs are the responsible for the excitation of the CMs. The main goal of the proposed approach is to control the excitation degree of the desired current modes (J_n) in order to place a null in the desired direction. Previous attempts succeeded only in placing the null only on the principal planes ($\phi = 0°, 90$) and within a limited angular sector ($\theta = \pm$ 30°). More in detail, the aim of this work is to demonstrate that a proper control of both the amplitude and phase of each CCE allows placing the null in any desired direction, even outside the principal planes. The key aspect is to place the exciters in the locations suggested by the Characteristic Modes Analysis (CMA) in order to excite the

The authors are with Dipartimento di Ingegneria dell'Informazione, University of Pisa, Pisa 56122, Italy (www.dii.unipi.it) and also with the CNIT, Parma 43124, Italy (www.cnit.it).

(e-mail: alessio.dicandia@for.unipi.it, simone.genovesi@unipi.it, agostino.monorchio@unipi.it).

necessary weighted combinations of orthogonal current modes (J_n). As a test case, the excitation of three characteristic modes on a rectangular plate with the size of a portable device will provide the evidence that the radiating structure is capable to place the pattern null in all directions of the upper hemisphere with a null depth greater than 27 dB. The measured results prove the reliability of the proposed approach that can be beneficial also for other platform geometries.

This paper is organized as follows. In Section II the CMs of the considered structure is addressed. Section III is devoted to illustrate the strategy used to choose the proper set of excitations applied to the CCEs that provides the pattern reconfigurable capability. Measurements on a fabricated prototype are illustrated in Section IV. Finally, the conclusions are reported in Section V.

II. Characteristic Modes Investigation

A description of the test case platform is illustrated in Fig. 1 with its geometrical dimensions. As a first step, the CMA of the rectangular plate is performed. The CMs analysis allows obtaining a set of orthogonal current modes (J_n) distribution that depend only from the antenna geometry, that are independent of any kind of external excitation [26]. Once these current modes (J_n) are known, the total current distribution (J_{tot}) over the investigated structure, can be decomposed as a liner superposition of these modes:

$$J_{tot} = \sum_k \alpha_k J_k \tag{1}$$

where α_k represents a complex coefficient related to the current mode J_k, generally known as modal weighing coefficient (MWC). Differently from the current modes (J_n), the MWC values are strongly influenced by the employed exciters. Therefore a proper choice of the exciters allows a selective excitation of the modes [27]. In other words, it is possible to implement a modal filtering by means of the external sources.

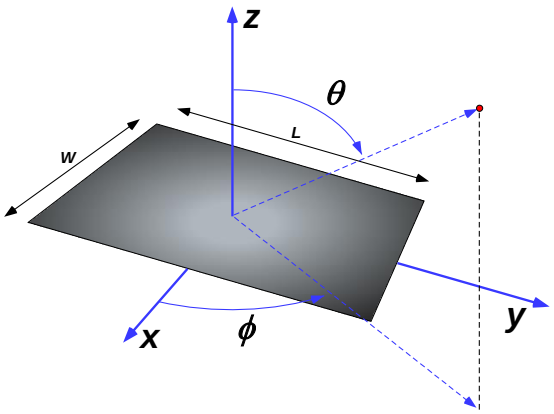

Fig. 1. Rectangular platform; L = 150 mm, W = 75 mm.

The eigenvalues (λ_n) related to the first ten modes of the rectangular conductive plane are shown in Fig. 2 as a function of the frequency. The eigenvalues are real numbers and a mode is considered at resonance when its associated value is equal to zero. This parameter is very important since it determines the reactive power related to each mode [28]. For this reason, a particular mode is easier to excite, and gives a greater contribute to the total radiated power, if its eigenvalue is close to zero. By observing Fig. 2, it is apparent that in the frequency range of interest, namely from 2.4 GHz to 2.5 GHz, the most of the modes have an eigenvalue magnitude lower than 2, except for Mode#7, Mode#9 and Mode#10 that are higher order modes. In particular, Mode#7 and#10 are identified as inductive modes ($\lambda > 0$), whereas Mode#9 is a capacitive mode ($\lambda < 0$). Therefore, in this frequency range these higher order modes do not give a significant contribution to the total radiated power. The current modes distribution (J_n) of the first ten modes, that the platform is able to support, are shown in Fig. 3.

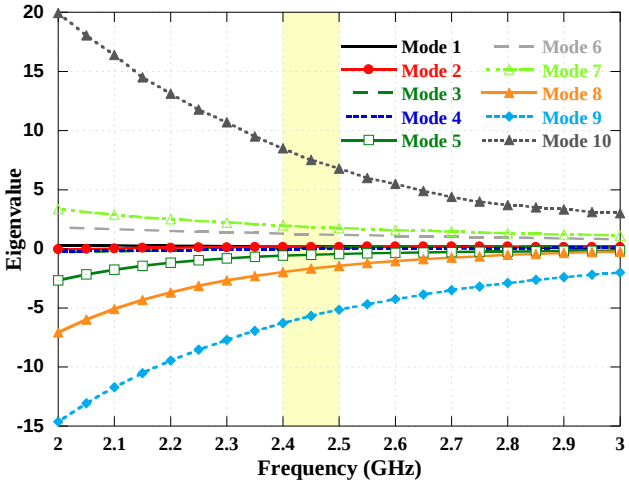

Fig. 2. Eigenvalues (λ_n) as a function of frequency.

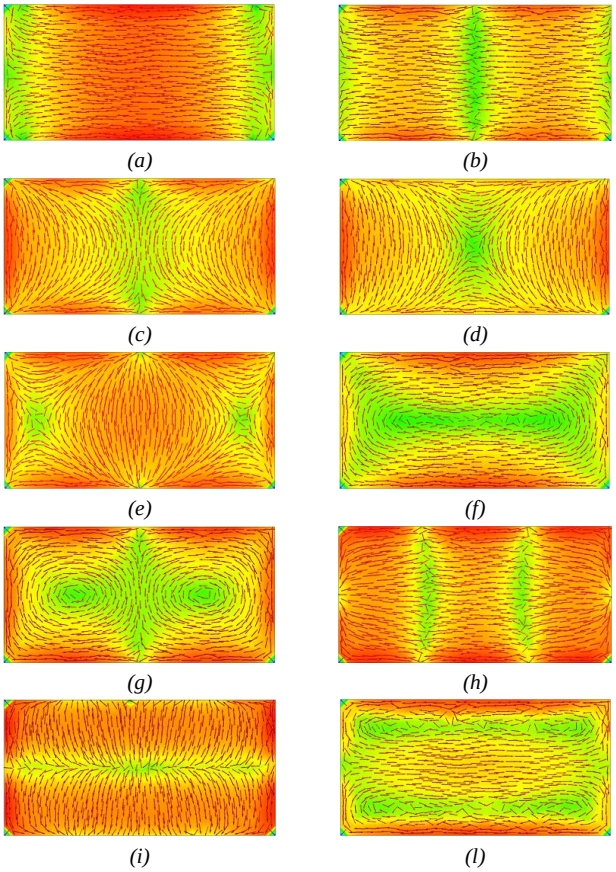

Fig. 3. Current distribution on the rectangular ground plane related to the mode number *(a)* 1, *(b)* 2, *(c)* 3, *(d)* 4, *(e)* 5, *(f)* 6, *(g)* 7, *(h)* 8, *(i)* 9, *(l)* 10.

It is evident that each mode presents a peculiar position of maxima and minima of the current and a different distribution as imposed by the CMT. It has been proved [23] that by employing two CCEs located in the middle of the short side, it is possible to excite Mode#2 and Mode#8 and generate a null of the pattern by exploiting a phase difference between the CCEs. However, the null of the pattern can be located in a limited θ angular sector and only on the *y*-*z* plane. From the inspection of the currents of these two modes (Fig. 3) it is apparent that they are mainly distributed along the *y*-direction and this fact limits the set of patterns that the structure can generate and the polarization of the radiated fields. The control of the patterns along other directions requires an additional degree of freedom that is represented by the excitation of another current distribution. The inspection the CMs is able to suggest not only the missing current distribution that has to be introduced, but also the exciter configuration to activate it.

In the considered example, a current distribution along *x*-direction would be beneficial for achieving a better null placement. For this reason, another couple of exciters is introduced in order to stimulate a current mode (J_n) mainly flowing along *x*-direction, such as Mode#5. The simplest way to achieve this is to place CCEs in the middle of the longest side as illustrated in Fig. 4. As it can be observed through the same Fig. 4, the four rectangular exciters are placed parallel to the sides of the rectangular plane at a height of 4 mm.

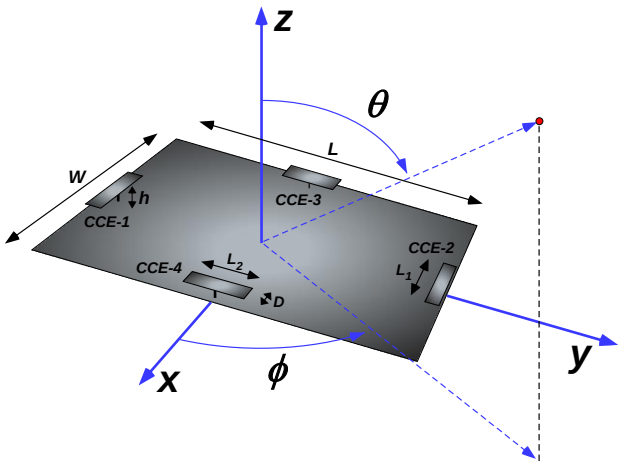

Fig. 4. Rectangular conductive plane with four capacitive exciters; L = 150 mm, W = 75 mm, L_1 = 33 mm, L_2 = 35 mm, D = 5 mm.

A voltage source between the ground plane and each CCE center has been introduced during the CMA in order to assess the excitation degree of the CMs by employing the capacitive sources. The normalized MWC amplitude analysis, performed when the CCEs are individually stimulated, helps to understand which current modes (J_n) are efficiently excited over the conductive plane within the frequency band of the operation (2.4 – 2.5 GHz). Fig. 5 shows that the couple of sources located along the *y*-axis (Port 1 and Port 2), are able to stimulate over the antenna both Mode#2 and Mode#8. On the contrary, the couple of CCEs hosted along the *x*-axis (Port 3 and Port 4), allows to efficiently stimulate both Mode#5 and Mode#2. Moreover, the level of the excitation of the other modes can be neglected since their normalized MWC amplitude is lower than 0.2. The lower amplitude of these modes is not surprising since they do not present a minimum of the current distribution nearby the exciters (Fig. 3) [24]. Therefore, the four CCEs excite Mode#2, Mode#5 and Mode#8 and hence the total current distribution over the antenna (J_{tot}) can be well approximated as a weighted combination of these three orthogonal current modes:

$$J_{tot} \cong \alpha_2 J_2 + \alpha_5 J_5 + \alpha_8 J_8 \qquad (2)$$

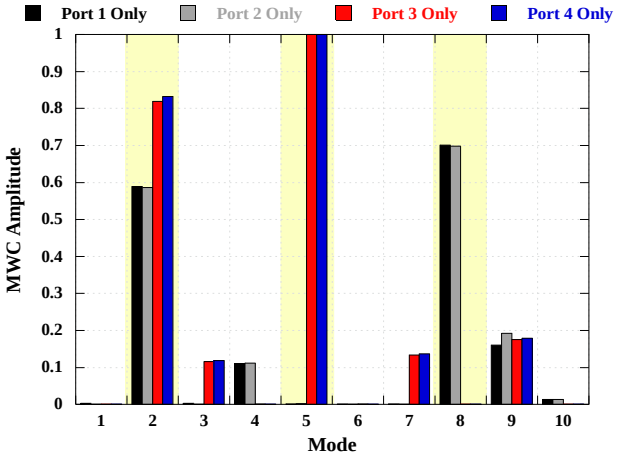

Fig. 5. Normalized amplitude of the MWC when the CCEs are individually excited at 2.45 GHz.

Furthermore, the excitation degree of the Mode#5 and Mode#8 depends only on the couple of sources located along *x*-axis and *y*-axis respectively, whereas the Mode#2 intensity is determined by all the four sources. The phase of the MWC related to each modes when the sources are individually excited are reported in Fig. 6. More in detail, the Fig. 6*a* shows the MWC phase when Port 1 and Port 2 are individually stimulated, whereas Fig. 6*b* presents the MWC phase when Port 3 and Port 4 are individually fed. The couple of CCEs located along the *y*-axis (Port1 and Port 2) excite Mode#2 with the same phase, whereas Mode#8 presents a phase difference of 180°. The same consideration can be also drawn for Port 3 and Port 4 regarding Mode#2 and Mode#5 (Fig. 6*b*). However, the MWC phase of Mode#2 is in opposition for the two couple of exciters.

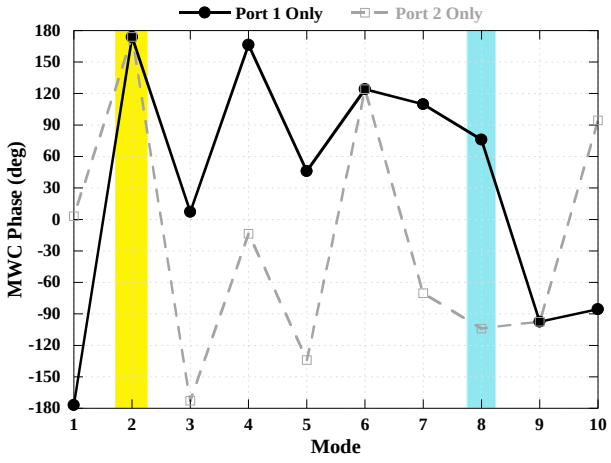

(a)

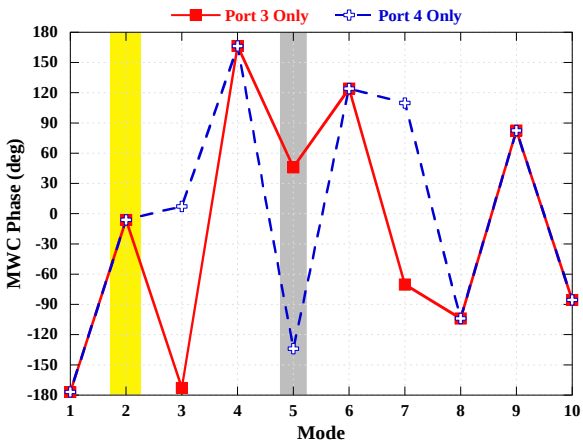

(b)

Fig. 6. Phase of the MWC when the CCEs are individually excited at 2.45 GHz; *(a)* CCE-1 and CCE-2, *(b)* CCE-3 and CCE-4.

The CMA shows, in a very effective way, the reason for which these three modes are stimulated by the probes, simply by observing the related current modes distribution (Fig. 7). Indeed, the CCEs are able to excite efficiently all the current modes (J_n) that present a minimum of the current modes distribution nearby the probes [24]. From Fig. 7, it can be noticed that both Mode#2 and Mode#8 (Fig. 7*a*-*c*) present a minimum of the current in the middle of the shortest side, whereas Mode#5 (Fig. 7*b*) has a current minima in the middle of the longest side. Therefore, since the CCE can excite only the current modes with current minima close to probe, the CCEs along the shorter side are able to stimulate over the antenna both the Mode#2 and Mode#8, whereas the CCEs along the longer side can stimulate efficiently both the Mode#5 and the Mode#2.

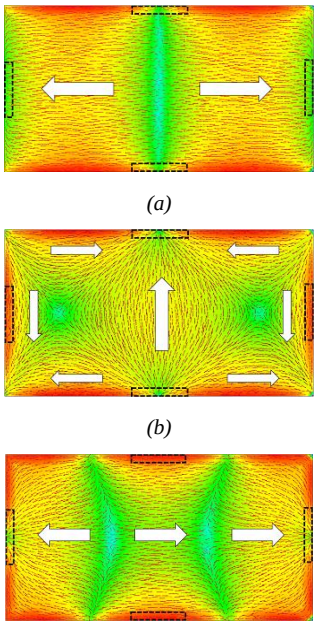

(a)

(b)

(c)

Fig. 7. Current mode distribution and the related normalized radiation pattern at 2.45 GHz of the *(a)* Mode#2, *(b)* Mode#5 and *(c)* Mode#8.

Furthermore, it is worth noting that any alteration of the investigated object affect the CMA by changing the eigenvalues behaviors with respect to the frequency and the current distribution of the modes over the object. However, the addition of small external exciters does not corrupt the CMA previously performed by considering only the rectangular conductive sheet, but only they generate a slight variation of the eigenvalues (λ_n) behavior with respect to the frequency. This concept is confirmed from Fig. 8 that compares the eigenvalues behaviors related to the three modes efficiently stimulated by CCEs by considering only the rectangular plane (RP) and the RP plus the CCEs (RP+CCEs).

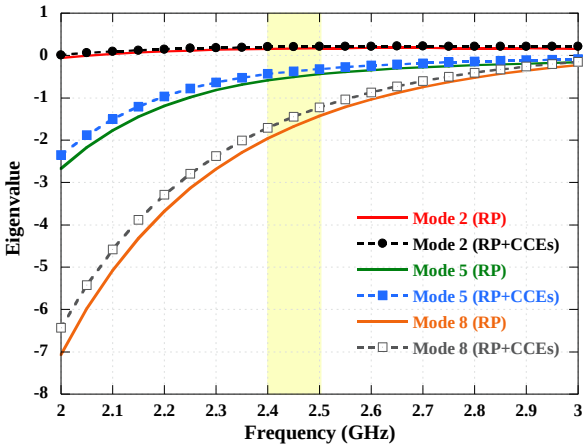

Fig. 8. Eigenvalues comparison related to Mode#2, Mode#5 and Mode#8 by considering only the rectangular plan e (RP) and the RP plus the CCEs.

Indeed, from the same Fig. 8, it is evident that the presence of the external CCEs introduce a slight alteration of the eigenvalues behaviors with respect to the frequency as expected. However, due to the small size of the CCEs with respect to the conductive plate dimension, the eigenvalues alteration can be neglected.

For the sake of completeness, in addition of the alteration of the eigenvalues behaviors with respect to the frequency due to the presence of the external exciters, the current modes (J_n) distributions related to Mode#2, Mode#5 and Mode#8 have been taken into account. In particular, Fig. 9 compares the current modes of the RP and the new current modes when the plate is loaded with CCEs. All the plots are represented on the same scale to ease the comparison.

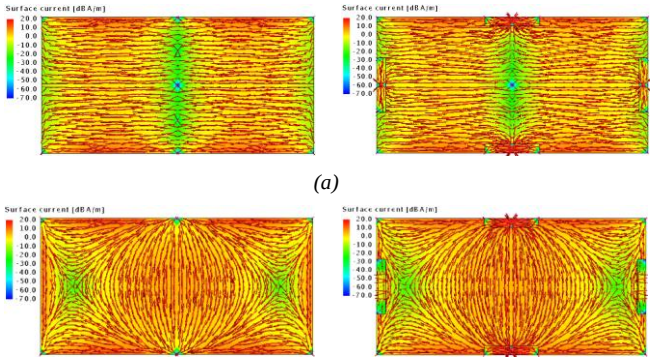

(a)

(b)

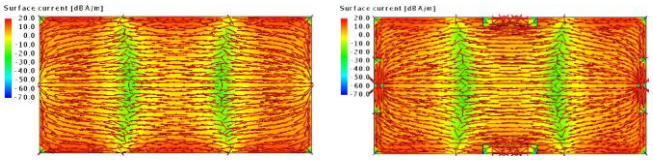

(c)

Fig. 9. Comparison of the current modes distribution by considering only the RP and the RP plus CCEs, *(a)* Mode#2, *(b)* Mode#5 and *(c)* Mode#8.

The good agreement between the currents observed in Fig. 9 with and without the CCEs confirms that the presence of external exciters does not corrupt the CMs analysis previously performed by considering only the conductive rectangular plate. Moreover, the radiation pattern of the modes with and without the CCE have been compared. The radiation pattern comparison related to Mode#2, Mode#5 and Mode#8 are illustrated in Fig. 10.

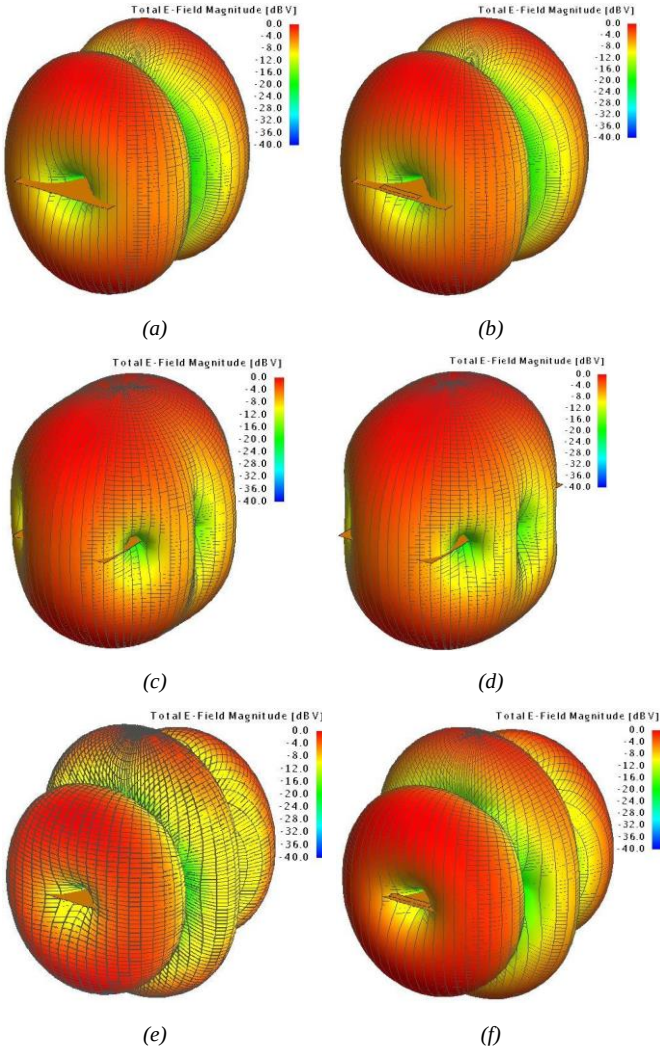

(a) *(b)* *(c)* *(d)* *(e)* *(f)*

Fig. 10. Modes radiation pattern comparison by considering only the RP and the RP+CCEs; *(a)* Mode#2 (RP), *(b)* Mode#2 RP+CCEs, *(c)* Mode#5 (RP), *(d)* Mode#5 (RP+CCEs), *(e)* Mode#8 (RP) and *(f)* Mode#8 (RP+CCEs).

In addition, the correlation values [28], [29] between the characteristic modes by considering the radiation patterns of the rectangular plane with and without the CCEs are reported in Table I. All the aforementioned results prove that the proposed CCEs does not affect the validity of the CMA performed initially on the original rectangular platform.

TABLE I
CORRELATION BETWEEN CMS BY CONSIDERING ONLY THE RP AND THE RP LOADED BY CCES

Mode#2	Mode#5	Mode#8
0.9994	0.9943	0.9986

III. NULL-SCANNING CAPABILITY

As previously shown, the four CCEs enable to excite efficiently over the conductive plane, only three current modes (J_n). For this reason, according to equation (1), the total current distribution (J_{tot}) can be approximated as a linear superposition of mainly three modes (2). In order to obtain a pattern reconfigurable antenna, the level of the excitation of the stimulated modes (α_n) [23] has to be properly tuned. By introducing a complex coefficient for each CCE (X_i, i=1, 2, 3, 4) and by defining $J^{(i)}$ as the total current distribution over the antenna due to the single exciter, the contribute of each source to the total current distribution (J_{tot}) can be expressed as:

$$\begin{cases} J^{(1)} = \sum_k X_1 \alpha_k^{(1)} J_k \cong X_1 \alpha_2^{(1)} J_2 + X_1 \alpha_8^{(1)} J_8 \\ J^{(2)} = \sum_k X_2 \alpha_k^{(2)} J_k \cong X_2 \alpha_2^{(2)} J_2 + X_2 \alpha_8^{(2)} J_8 \\ J^{(3)} = \sum_k X_3 \alpha_k^{(3)} J_k \cong X_3 \alpha_2^{(3)} J_2 + X_3 \alpha_5^{(3)} J_5 \\ J^{(4)} = \sum_k X_4 \alpha_k^{(4)} J_k \cong X_4 \alpha_2^{(4)} J_2 + X_4 \alpha_5^{(4)} J_5 \end{cases} \quad (3)$$

where $\alpha_k^{(i)}$ represents the normalized MWC calculated in the previous section related to the k^{th} current mode of the i^{th} exciter and X_i is a complex value with a magnitude within [0,1] and a phase between -180° and 180°. If we define with $J^{(1\text{-}2)}$ and $J^{(3\text{-}4)}$ the current distribution over the antenna due to the couple of the sources located along the *y*-axis and *x*-axis, respectively, the total current distribution (J_{tot}) can be written as:

$$\begin{cases} J_{tot} = J^{(1-2)} + J^{(3-4)} \\ J^{(1-2)} \cong \left(X_1 \alpha_2^{(1)} + X_2 \alpha_2^{(2)} \right) J_2 + \left(X_1 \alpha_8^{(1)} + X_2 \alpha_8^{(2)} \right) J_8 \\ J^{(3-4)} \cong \left(X_3 \alpha_2^{(3)} + X_4 \alpha_2^{(4)} \right) J_2 + \left(X_3 \alpha_5^{(3)} + X_4 \alpha_5^{(4)} \right) J_5 \end{cases} \quad (4)$$

From Fig. 11 it is apparent the effect of changing the level of the excitation of the current modes. Indeed, by manipulating both the magnitude and phase of the four feeding ports (X_i), it is possible to alter the MWC values and thus the total current distribution (J_{tot}).

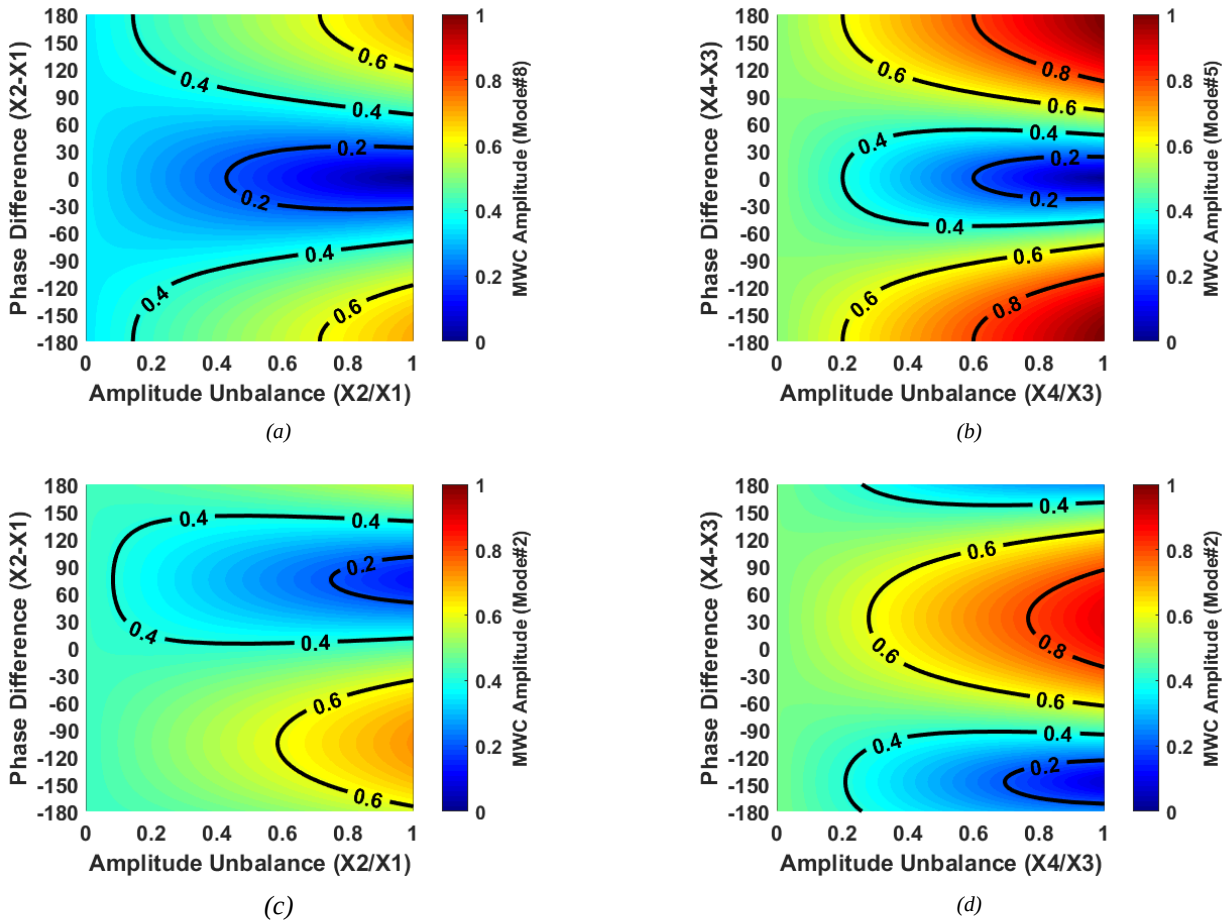

Fig. 11. Normalized MWC amplitude as a function of the amplitude unbalance and phase difference between the sources. *(a)* Mode #8 intensity with respect to the sources 1-2, *(b)* Mode #5 intensity with respect to the sources 3-4, *(c) Mode #2* intensity with respect to the sources 1-2 when $X_3 = 1e^{j90°}$ and $X_4 = 1e^{j0}$, *(d)* Mode #2 intensity with respect to the sources 3-4 when $X_1 = 0.5e^{j180°}$ and $X_2 = 1^{e-j60°}$.

In order to better understanding the change of the MWC due to different feedings, the MWC amplitude is illustrated in Fig. 11 as a function of both amplitude and phase manipulation. It is apparent that the MWC amplitude strongly depends on the external feeding ports. Indeed, the desired combination of the current modes, useful to satisfy a desired radiation pattern requirement, can be obtained by a proper feeding. More in detail, Mode#5 and Mode#8 are influenced only by the couple of the CCEs located along the *x*-axis (CCE-3 and CCE-4) and *y*-axis (CCE- 1 and CCE-2) respectively, whereas Mode#2 depends on all the ports simultaneously. Therefore, to underline this aspect, the MWC related to Mode#2, has been evaluated by considering two different configurations of the feedings (Fig. 11*c*-*d*). In particular, the Fig. 11*c* shows the MWC intensity as a function of the CCE-1 and CCE- 2, whereas in the Fig. 11*d* it is reported the MWC intensity with respect to the CCE-3 and CCE-4. In these two above-mentioned cases, the other ports are fed with a constant value. More in detail, the Mode#8 intensity is strongly stimulated when Port 1 and Port 2 are out-of-phase and present the same amplitude level (Fig. 11*a*). However, by decreasing the phase difference, the Mode#8 intensity gradually decreases until it vanishes when the probes along the *y*-axis are fed in-phase and with the same amplitude level. Moreover, by introducing some amplitude unbalance between the probes, the MWC intensity undergoes a more gradual alteration with respect to the phase difference. The same behavior remains valid also for Mode#5 (Fig. 11*b*) by means of CCE-3 and CCE- 4.

The described MWC behavior with respect to the feeding ports manipulation is at the basis at of the null-scanning propriety of the proposed antenna. Through the feeding ports manipulation presented in Fig. 11, it is possible to individually excite the three current modes (J_2, J_5 and J_8) or achieve a weighted combination of these currents modes. As an example, the simulated total current distribution on the antenna for different values of the feeding ports (X_i) is shown in Fig. 12. The excitation of each single mode (Fig. 12*a*, *b*, *c*) as well as an example of a weighed current distribution (Fig. 12*d*) obtained from a linear combination according to (4), are illustrated.

By summarizing, the first step requires the knowledge of the current modes (J_n): this task can be accomplished by the CMA. The inspection of the different modal currents provides the indication of the modes that have to be excited. Next, the CMA also suggests the suitable place and kind of exciters. Finally, the controlled excitation (X_i) of the external probes allows the fulfillment of the desired requirements in term of radiated power. This concept can be exploited for any platform geometry in order to achieve a three dimensional null-placing antenna.

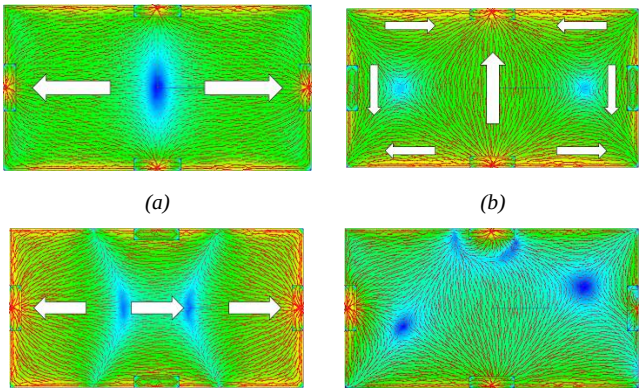

(a) *(b)* *(c)* *(d)*

Fig. 12. Total current distribution on the antenna by changing the feeding ports; *(a)* $X_1 = 1e^{j0°}$, $X_2 = 1e^{j0°}$, $X_3 = X_4 = 0$, *(b)* $X_1 = X_2 = 0$, $X_3 = 1e^{j0°}$, $X_4 = 1e^{j180°}$, *(c)* $X_1 = 1e^{j0°}$, $X_2 = 1e^{j180°}$, $X_3 = X_4 = 0$, *(d)* $X_1 = 1e^{j0°}$, $X_2 = 0.5e^{j90°}$, $X_3 = 0.6e^{j180°}$, $X_4 = 1e^{j30°}$.

The required input port feeding (X_i), necessary to provide a set of the MWCs able to produce a null of the pattern in the desired direction, has been evaluated by solving the linear equation:

$$\underline{E}_{tot}(r,\theta,\phi) = \sum_i \sum_k X_i \alpha_k^{(i)} \underline{E}_k(r,\theta,\phi) = 0 \qquad (5)$$

where $\underline{E}_k(r,\theta,\phi)$ represents the electric field related to the k^{th} CM in the direction $P(\theta,\phi)$, $\alpha_k^{(i)}$ the MWC of the k^{th} CM related to the i^{th} CCE and the $\underline{E}_{tot}(r,\theta,\phi)$ the total electric field radiated from the antenna in the direction $P(\theta,\phi)$. The simulated normalized radiation patterns obtained by solving (5) for different directions of the null are shown in Fig. 13. In particular, in Fig. 13*a*-*b* the radiation pattern along the principal planes ($\phi = 0°$ and $\phi = 90°$) are reported, whereas in Fig. 13*c* the results for plane $\phi = 45°$ are shown. As apparent, the proposed antenna is capable to place a null of the pattern in all the desired directions with a remarkable null-depth. It is worthwhile noting that the null-scanning capability is also verified for all the other (θ,ϕ) directions, but for the sake of brevity, they are not reported here.

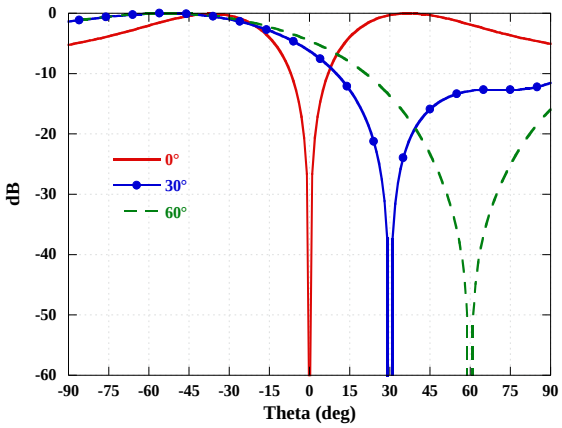

(a)

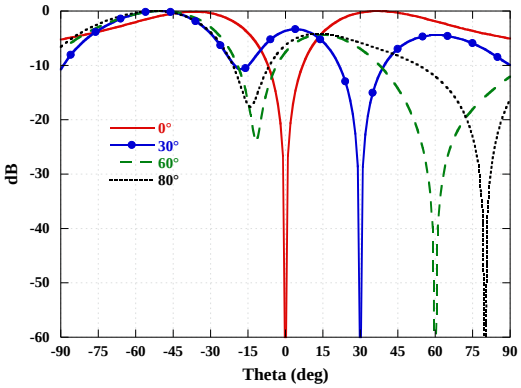

(b)

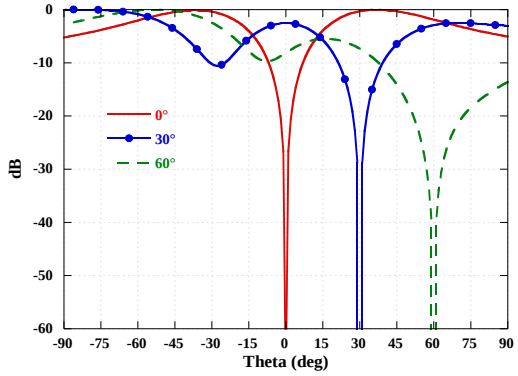

(c)

Fig. 13. Simulated normalized radiation pattern at 2.45 GHz; *(a)* $\phi = 0°$, *(b)* $\phi = 90°$, *(c)* $\phi = 45°$.

A. *Discrete Source Model*

As previously shown through Fig. 13, by taking into account an ideal feeding with an infinite resolution in terms of power unbalance and phase difference among the CCEs, the proposed design strategy is able to provide an optimal weight for each current mode useful to place a pattern null in any direction with an infinite Null-Depth. However, in a real life scenario, the feeding network is able to provide only discrete values regarding the power unbalance and phase difference among the CCEs. For this reason, in order to prove the reliability of the proposed strategy, the three dimensional null-scanning capability is evaluated by taking into account real commercially available components. In particular, a discrete source model has been applied for each CCE feeding over the rectangular plane. A four-bit broadband digital attenuator (SKY12348-350LF) has been considered, with a maximum power attenuation of 15 dB and a step of 1dB. Regarding the phase difference, a Reflection Type Phase Shifter (RTFS) with a 360° phase shifter [30] with a step of 10° has been adopted.

The three dimensional null-scanning capability with these COTS tunable components is assessed by analyzing the Null-Depth in the entire upper hemisphere and the result is reported in Fig. 14*a*. Moreover, to achieve a statistical characterization of the obtained performance, the Cumulative distribution Function (C.d.F) of the Null-Depth is evaluated and it is reported in Fig. 14*b*. As it is evident, the proposed design strategy allows obtaining a remarkable Null-Depth in any

direction of the upper hemisphere even by considering commercially available components. Obviously, with the increasing (decreasing) of the phase shifters and attenuators performance, there is an improvement (deterioration) of the proposed antenna statistical performance. For comparison, a Normal distribution with the same mean and variance of the Null-Depth distribution is reported in Fig. 14*b*. The good matching between the curves prove that the Null-Depth distribution in the entire upper hemisphere is almost coincident with a Normal distribution. Table II summarizes the statistical behavior of the three dimensional null-scanning in terms of mean value of the Null-Depth (η) and the probability that the Null-Depth is lower of – 25 dB. Table II reveals a mean value of the Null-Depth equal to – 32 dB and a probability of 0.96 to achieve a Null-Depth lower than – 25 dB.

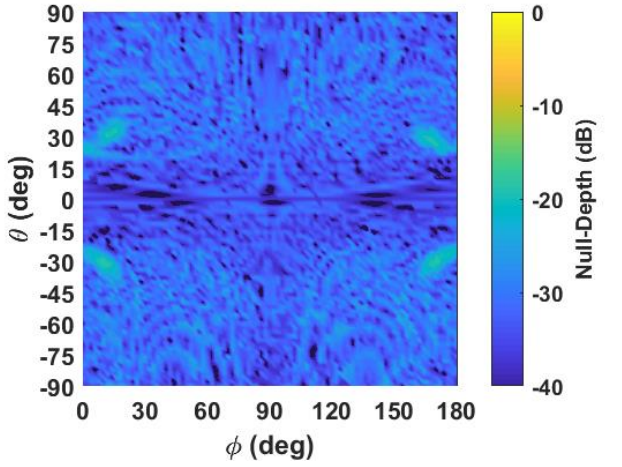

(a)

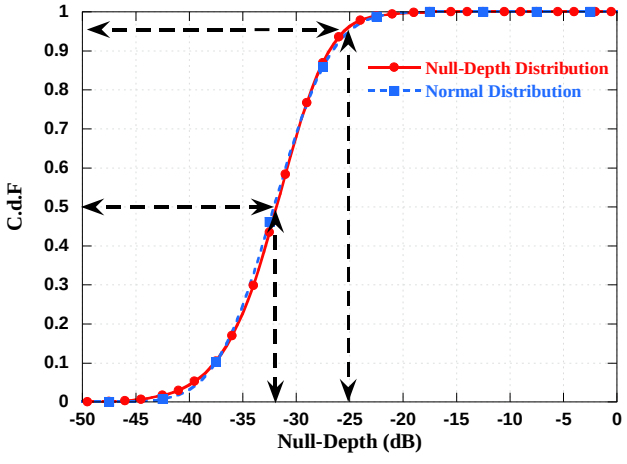

(b)

Fig. 14. *(a)* Three dimensional Null-Depth in entire upper hemisphere and the *(b)* Cumulative distribution Function (C.d.F) of the Null-Depth.

TABLE II
STATISTICAL CHARACTERIZATION OF THE THREE DIMENSIONAL NULL-SCANNING CAPABILITY WITH REAL COMPONENTS

Null-Depth mean (η)	Pr (Null-Depth < – 25 dB)
–32 dB	0.96

IV. PROTOTYPE AND MEASUREMENTS

In order to assess the simulated performance, a prototype of the structure, with the appropriate feeding network, has been manufactured on a grounded dielectric layer (FR4) (Fig. 15). The presence of the dielectric layer does not affect the CMs analysis performed in the previous section [19]. The length of the exciters (L_1 and L_2) has been selected for having an input impedance almost real in the frequency range of operation. In order to efficiently match the CCEs to the 50 Ω of the feeding network microstrip lines, a quarter wavelength impedance transformer has been employed for each CCEs.

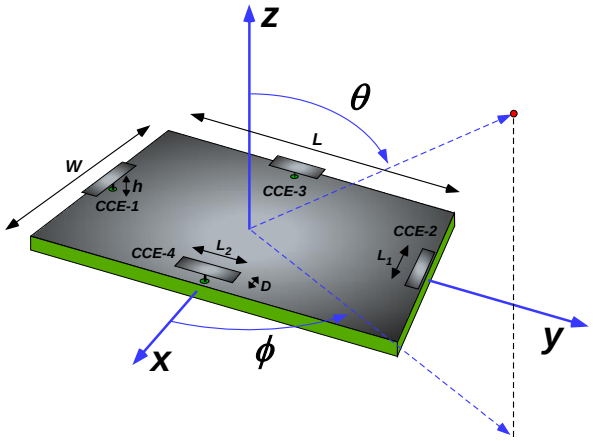

Fig. 15. Rectangular conductive sheet placed on a substrate dielectric layer.

A sketch of the overall antenna system is shown in Fig. 16. It consists of the rectangular conductive plane with four ports and an external feeding network. The input port feeding (X_i) are obtained by a proper power attenuation and phase shift in order to satisfy the null-scanning requirement found by using (5).

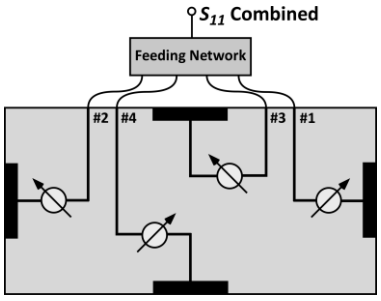

Fig. 16. Overall antenna system.

The manufactured prototype of the proposed null-scanning antenna is reported in Fig. 17. The CCEs are printed on a FR4 single-sided copper substrate with the same thickness of 1.2 mm of the conductive sheet. They are connected to the feeding network through a via connection. In order to keep the exciters at the exact height of 4 mm from the ground plane and make them more robust, a foam spacer has been also employed. The four ports of the conductive plane have been connected to the four output ports of the external feeding network, which comprise three Wilkinson power dividers (Fig. 17*c*). The overall antenna system is illustrated in Fig. 17*d*. The feeding network consists of a Reflection Type Phase Shifter (RTPS) [31], realized with an a hybrid junction (HJ) with two ports closed on a reactive load, and an attenuator realized with a

variable pi-network of resistors [32]. These two microwave components are employed for each of the four ports to be able to provide the required amplitude unbalance and phase shift between the four exciters of the investigated antenna (Fig. 17*b*). In order to make the realization process simpler, all soldered components in the feeding network have a fixed value and are not variable. For this reason, the effectiveness of this design strategy has been proved by changing the components and by manufacturing several prototypes. It is important underline that the manufactured prototypes are employed only with the purpose of comparing simulations and measurements and thus assess the reliability of our design strategy. As a matter of fact, the prototypes used in our measurements campaign are not meant to be employed in a commercial device since the feeding network is not tunable. Hence, the load of the RTPS and the power attenuators have to exhibit tunable values to achieve the three dimensional null-scanning capability with a single feeding network.

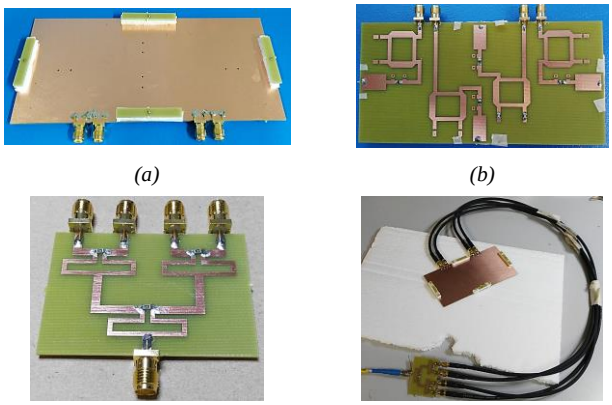

(a) *(b)* *(c)* *(d)*

Fig. 17. Prototype of the manufactured antenna; *(a)* radiating element with the four CCEs, *(b)* feeding network below the substrate dielectric layer, *(c)* external feeding network to provide four equal signal and *(d)* overall antenna system.

At the beginning, the external feeding network, which comprises three Wilkinson power dividers (WPDs) and the single RTPS have been characterized and measured. The measured magnitude and phase of the input reflection coefficient (S_{11}) and the transmission coefficient (S_{ij}) of the WPDs as well as the RTPS are illustrated in Fig. 18.

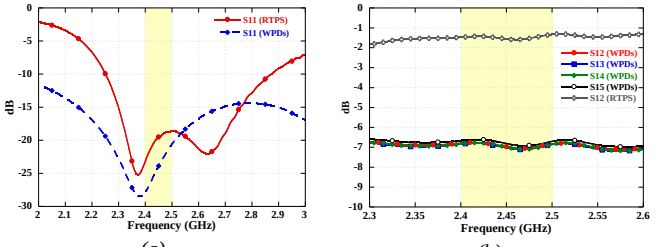

(a) *(b)*

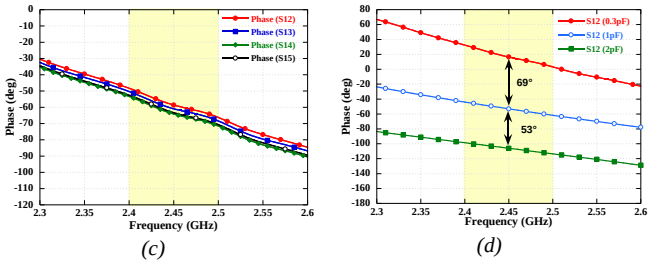

(c) *(d)*

Fig. 18. Measured *(a)* input reflection coefficient (S_{11}) and *(b)* transmission coefficient (S_{ij}) of the WPDs and RTPS. S_{ij} Phase *(c)* of the WPDs and *(d)* RTPS as a function of different capacitor.

In Fig. 19 the comparison between the simulated and the measured reflection coefficient (S_{ii}) of the four exciters is reported when the null is placed in direction ($\phi = 90°$ and $\theta = 60°$). The agreement between simulations and measurements is satisfactory. Obviously, for each configuration of the feeding network (X_i), the S_{ii} parameters exhibit a slight changing. However, the antenna input ports maintain a good matching within the frequency band of operation (2.4 GHz-2.5 GHz).

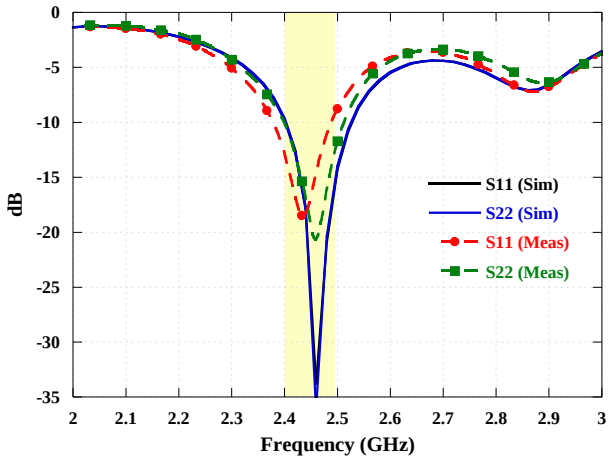

(a)

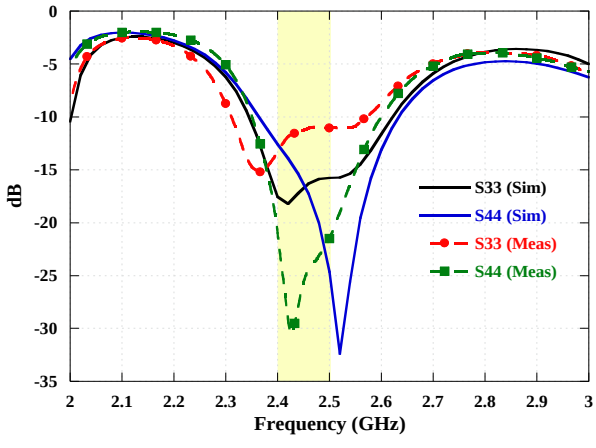

(b)

Fig. 19. Comparison between the simulated and measured S_{ii} parameters as a function of the frequency; *(a)* S_{11} and S_{22}, *(b)* S_{33} and S_{44} of the conductive plane when the null is placed in direction ($\phi = 90°$ and $\theta = 60°$).

The comparison between the simulated and the measured overall S_{11} (the *combined* S_{11} in Fig. 16) is reported in Fig. 20, which highlights a quite good matching within the frequency band of interest (2.4GHz-2.5 GHz).

Finally, the comparisons between simulated and measured normalized radiation patterns in the principal planes ($\phi = 0°$ and $\phi = 90°$) and for $\phi = 45°$ are presented in Fig. 21 for different null directions.

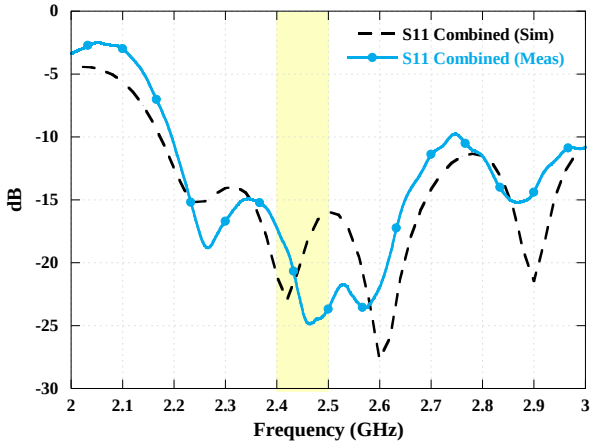

Fig. 20. Comparison between the simulated and measured S_{11} combined of the overall antenna system.

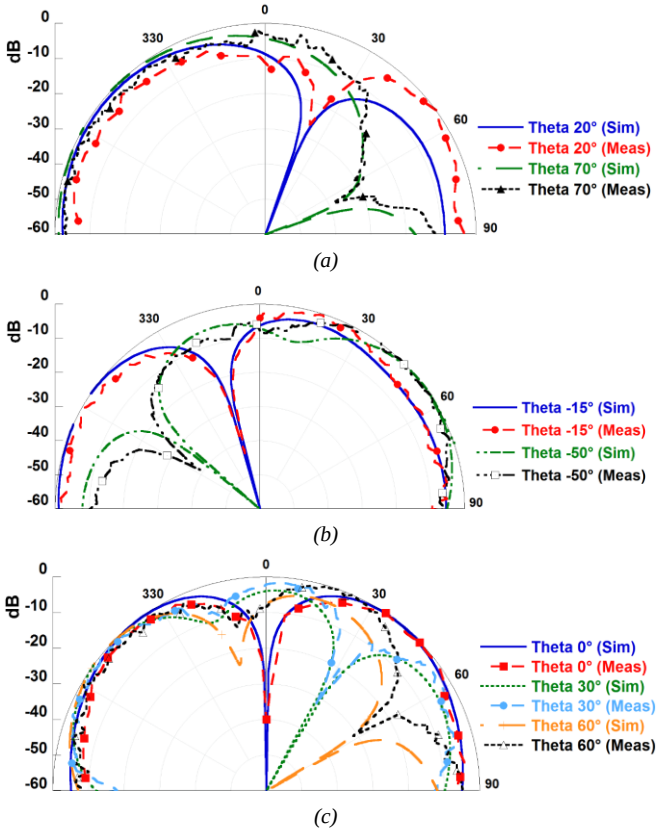

(a)

(b)

(c)

Fig. 21. Comparison between simulated and measured normalized radiation pattern at 2.45 GHz; *(a)* $\phi = 0°$, *(b)* $\phi = 45°$, *(c)* $\phi = 90°$.

The measured radiation patterns are in good agreement with the simulations and this confirms the reliability of the described design process. In particular, it is possible to achieve a three dimensional null-scanning antenna with a measured null-depth greater than 27 dB. The obtained results in terms of scan angle and null-depth are summarized in Table III.

TABLE III
MEASURED SCAN ANGLE AND NULL-DEPTH AT 2.45 GHz

Desired angles ϕ, θ (deg)	Scan-angle (deg)	Null-depth (dB)
0, 20	0, 22	27
0, 70	0, 65	38
45, -15	45, -15	43
45, -50	45, -56	39
90, 0	90, 0	40
90, 20	90, 19	32
90, 60	90, 57	31

V. CONCLUSION

A novel design strategy for placing a null of the pattern of a reconfigurable antenna in any desired direction has been proposed. A rigorous CMA of the considered radiating structure supports the described approach. The results of the CMA provides the information about the kind of exciters and their placement on the considered platform. By exploiting the amplitude unbalance between the exciters, as well as the phase difference, it is possible to obtain a MWC intensity alteration, which is at the basis of investigated null-scanning capability. As a test case, the guidelines for the excitation of three characteristic modes on a rectangular plate by means of four CCEs have been described. The three dimensional null-scanning capability by employing a discrete source model, which mimics real COTS components, has been assessed by analyzing the three dimensional Null-Depth in the entire upper hemisphere. Moreover, a statistical characterization is achieved by means of C.d.F of the Null-Depth.

In order to prove the null-scanning capability by exploiting the MWC alteration, a prototype of the antenna has been realized and tested. The measured and simulated results present a good agreement and confirm the reliability of the described design process based on the CMA.

REFERENCES

[1] C. G. Christodoulou, Y. Tawk, S. A. Lane, and S. R. Erwin, "Reconfigurable Antennas for Wireless and Space Applications," *Proc. IEEE*, vol. 100, no. 7, pp. 2250–2261, Jul. 2012.

[2] S. Genovesi, A. D. Candia, and A. Monorchio, "Compact and Low Profile Frequency Agile Antenna for Multistandard Wireless Communication Systems," *IEEE Trans. Antennas Propag.*, vol. 62, no. 3, pp. 1019–1026, Mar. 2014.

[3] S. Genovesi, A. Monorchio, M. B. Borgese, S. Pisu, and F. M. Valeri, "Frequency-Reconfigurable Microstrip Antenna With Biasing Network Driven by a PIC Microcontroller," *IEEE Antennas Wirel. Propag. Lett.*, vol. 11, pp. 156–159, 2012.

[4] H. L. Zhu, S. W. Cheung, X. H. Liu, and T. I. Yuk, "Design of Polarization Reconfigurable Antenna Using Metasurface," *IEEE Trans. Antennas Propag.*, vol. 62, no. 6, pp. 2891–2898, Jun. 2014.

[5] G. H. Huff and J. T. Bernhard, "Integration of Packaged RF MEMS Switches With Radiation Pattern Reconfigurable Square Spiral Microstrip Antennas," *IEEE Trans. Antennas Propag.*, vol. 54, no. 2, pp. 464–469, Feb. 2006.

[6] B. A. Cetiner, H. Jafarkhani, J.-Y. Qian, H. J. Yoo, A. Grau, and F. De Flaviis, "Multifunctional reconfigurable MEMS integrated antennas for adaptive MIMO systems," *Commun. Mag. IEEE*, vol. 42, no. 12, pp. 62–70, 2004.

[7] Z. Li, E. Ahmed, A. M. Eltawil, and B. A. Cetiner, "A Beam-Steering Reconfigurable Antenna for WLAN Applications," *IEEE Trans. Antennas Propag.*, vol. 63, no. 1, pp. 24–32, Jan. 2015.

[8] I. Lim and S. Lim, "Monopole-Like and Boresight Pattern Reconfigurable Antenna," *IEEE Trans. Antennas Propag.*, vol. 61, no. 12, pp. 5854–5859, Dec. 2013.

[9] S. Yong and J. T. Bernhard, "A Pattern Reconfigurable Null Scanning Antenna," *IEEE Trans. Antennas Propag.*, vol. 60, no. 10, pp. 4538–4544, Oct. 2012.

[10] S. Yong and J. T. Bernhard, "Reconfigurable Null Scanning Antenna With Three Dimensional Null Steer," *IEEE Trans. Antennas Propag.*, vol. 61, no. 3, pp. 1063–1070, Mar. 2013.

[11] X. Jiang, Z. Zhang, Y. Li, and Z. Feng, "A Novel Null Scanning Antenna Using Even and Odd Modes of a Shorted Patch," *IEEE Trans. Antennas Propag.*, vol. 62, no. 4, pp. 1903–1909, Apr. 2014.

[12] C. Deng, Y. Li, Z. Zhang, and Z. Feng, "A Hemispherical 3-D Null Steering Antenna for Circular Polarization," *IEEE Antennas Wirel. Propag. Lett.*, vol. 14, pp. 803–806, 2015.

[13] R. Harrington and J. Mautz, "Theory of characteristic modes for conducting bodies," *IEEE Trans. Antennas Propag.*, vol. 19, no. 5, pp. 622–628, Settembre 1971.

[14] R. Garbacz and R. Turpin, "A generalized expansion for radiated and scattered fields," *IEEE Trans. Antennas Propag.*, vol. 19, no. 3, pp. 348–358, Maggio 1971.

[15] D. Manteuffel and R. Martens, "Compact Multi Mode Multi Element Antenna for Indoor UWB Massive MIMO," *IEEE Trans. Antennas Propag.*, pp. 1–1, 2016.

[16] M. Bouezzeddine and W. L. Schroeder, "Design of a Wideband, Tunable Four-Port MIMO Antenna System With High Isolation Based on the Theory of Characteristic Modes," *IEEE Trans. Antennas Propag.*, vol. 64, no. 7, pp. 2679–2688, Jul. 2016.

[17] C. Deng, Z. Feng, and S. V. Hum, "MIMO Mobile Handset Antenna Merging Characteristic Modes for Increased Bandwidth," *IEEE Trans. Antennas Propag.*, pp. 1–1, 2016.

[18] K. Kumar Kishor and S. V. Hum, "A Pattern Reconfigurable Chassis-Mode MIMO Antenna," *IEEE Trans. Antennas Propag.*, vol. 62, no. 6, pp. 3290–3298, Jun. 2014.

[19] H. Li, Z. T. Miers, and B. K. Lau, "Design of Orthogonal MIMO Handset Antennas Based on Characteristic Mode Manipulation at Frequency Bands Below 1 GHz," *IEEE Trans. Antennas Propag.*, vol. 62, no. 5, pp. 2756–2766, May 2014.

[20] T.-Y. Shih and N. Behdad, "Bandwidth Enhancement of Platform-Mounted HF Antennas Using the Characteristic Mode Theory," *IEEE Trans. Antennas Propag.*, pp. 1–1, 2016.

[21] Y. Chen and C.-F. Wang, "HF Band Shipboard Antenna Design Using Characteristic Modes," *IEEE Trans. Antennas Propag.*, vol. 63, no. 3, pp. 1004–1013, Mar. 2015.

[22] Y. Chen and C.-F. Wang, "Electrically Small UAV Antenna Design Using Characteristic Modes," *IEEE Trans. Antennas Propag.*, vol. 62, no. 2, pp. 535–545, Feb. 2014.

[23] F. A. Dicandia, S. Genovesi, and A. Monorchio, "Null-Steering Antenna Design Using Phase-Shifted Characteristic Modes," *IEEE Trans. Antennas Propag.*, vol. 64, no. 7, pp. 2698–2706, Jul. 2016.

[24] R. Valkonen, A. Lehtovuori, and D. Manteuffel, "Capacitive coupling elements—Changing the way of designing antennas," in *Antennas and Propagation (EuCAP), 2014 8th European Conference on*, 2014, pp. 229–233.

[25] R. Valkonen, M. Kaltiokallio, and C. Icheln, "Capacitive Coupling Element Antennas for Multi-Standard Mobile Handsets," *IEEE Trans. Antennas Propag.*, vol. 61, no. 5, pp. 2783–2791, May 2013.

[26] H. Li, Y. Tan, B. K. Lau, Z. Ying, and S. He, "Characteristic Mode Based Tradeoff Analysis of Antenna-Chassis Interactions for Multiple Antenna Terminals," *IEEE Trans. Antennas Propag.*, vol. 60, no. 2, pp. 490–502, Feb. 2012.

[27] R. Martens, E. Safin, and D. Manteuffel, "Selective excitation of characteristic modes on small terminals," in *Antennas and Propagation (EUCAP), Proceedings of the 5th European Conference on*, 2011, pp. 2492–2496.

[28] E. Safin and D. Manteuffel, "Reconstruction of the Characteristic Modes on an Antenna Based on the Radiated Far Field," *IEEE Trans. Antennas Propag.*, vol. 61, no. 6, pp. 2964–2971, Jun. 2013.

[29] D. Manteuffel and R. Martens, "Systematic design method of a mobile multiple antenna system using the theory of characteristic modes," *IET Microw. Antennas Propag.*, vol. 8, no. 12, pp. 887–893, Sep. 2014.

[30] O. D. Gurbuz and G. M. Rebeiz, "A 1.6-2.3 GHz RF MEMS Reconfigurable Quadrature Coupler and Its Application to a 360° Reflective-Type Phase Shifter," *IEEE Trans. Microw. Theory Tech.*, vol. 63, no. 2, pp. 414–421, Feb. 2015.

[31] C.-S. Lin, S.-F. Chang, C.-C. Chang, and Y.-H. Shu, "Design of a Reflection-Type Phase Shifter With Wide Relative Phase Shift and Constant Insertion Loss," *IEEE Trans. Microw. Theory Tech.*, vol. 55, no. 9, pp. 1862–1868, Sep. 2007.

[32] S. Otto, A. Bettray, and K. Solbach, "A distributed attenuator for K-band using standard SMD thin-film chip resistors," in *2009 Asia Pacific Microwave Conference*, 2009, pp. 2148–2151.